Iraqi Geological Journal

Journal homepage: https://www.igj-iraq.org

Red Clay Soil Physical and Chemical Properties Distribution Using Remote Sensing and GIS Techniques in Kirkuk City, Iraq

Veyan F. Salahalden[1,*], Muntadher A. Shareef [1] and Qahtan A. Al Nuaimy[1]

[1] Surveying Engineering Departement, Technical Engineering College- Kirkuk, Northern Technical University, Mosul, Iraq

* **Correspondence**: veyan.farhad@ntu.edu.iq

Received:
1 July 2023

Accepted:
18 October 2023

Published:
31 January 2024

Abstract

This research focuses on the study of the physical and chemical properties of red clay found in the Injana and Fatha Formations. The aim is to establish correlations among various physical and chemical elements using geographic information system (GIS), remote sensing, and a regression analysis model. Laboratory analysis, including X-ray diffraction, was conducted to determine the properties of the clay, as well as nonclay minerals. Statistical Package for the Social Sciences software was utilized for regression analysis to determine property correlations. Landsat 7 and Landsat 8 images were employed to establish relationships between digital numbers and soil properties. The study revealed that the dry density of the Fatha Formation was lower than that of the Injana Formation. Silt content was highest among all samples, ranging from 28% to 93%. The Fatha Formation exhibited a high gypsum rate due to the presence of gypsum layers. Strong positive correlations were observed between gypsum and sulfate, as well as between electrical conductivity and total soluble salt. Multiple linear regression analysis was appropriate for clay properties, with regression coefficients ranging from 0.6 to 0.72. Nonlinear regression yielded better results than linear regression, with high regression coefficients. Landsat images proved valuable for obtaining data in remote or expansive areas. The association between clay characteristics and Landsat 8 provided superior results compared to Landsat 7.

Keywords: Clay; Remote sensing ; Physical and chemical properties; XRD ; Injana and Fatha formations

1. Introduction

Clay, a widely abundant natural mineral (Ismail and Omar, 2014), includes red clay, a reddish-brown to yellow clay resulting from the chemical weathering of carbonate rocks under conditions of moderate temperature and high humidity (Zhang et al., 2020). Its unique physical and chemical properties have made clay indispensable in various aspects of our daily lives. Clay has been utilized by humans since ancient times and continues to play a significant role in diverse industries, such as ceramics, construction materials, healthcare, agriculture, civil engineering, environmental management, and the chemical industry (Moreno-Maroto and Alonso-Azcárate, 2018, Surdashy and Aqrawi, 2021, Ali et al., 2023). Conducting soil property mapping in remote areas is challenging, and traditional survey methods can be costly (McBratney et al., 2003, Akumu et al., 2015). However, the advent of Geographic Information System (GIS), remote sensing (RS), and modelling techniques has provided valuable tools for predicting soil properties across landscapes, even in previously inaccessible regions (Shareef et al., 2020b, Maarez et al., 2022). Therefore, there is an increasing need and desire to employ technologies

DOI: 10.46717/igj.57.1A.16ms-2024-1-27

such as GIS, RS, and modelling techniques to predict soil properties across landscapes (McBratney et al., 2003, Akumu et al., 2015, Shareef et al., 2020a). GIS enables the creation of high-resolution soil maps, surpassing the capabilities of traditional survey methods (Nkwunonwo and Okeke, 2013, Akumu et al., 2015, Hasan et al., 2021). RS imagery has proven effective in accurately and swiftly estimating soil parameters (Liao et al., 2013, Salahalden et al., 2023). Due to the importance of studying the physical and chemical properties of the soil and predicting these properties, researchers have used several methods, such as the studies (Martins and Gadiga, 2015), which suggested that the image's false colour composite (FCC) was created using band rationing (5/7:5/4:3/1) RGB by using Landast 7 to identify the spectral reflectance of a mineral deposit. The authors studied the chemical properties of soil by using gamma and neutron radiation and inductively coupled plasma–mass spectrometry (Taqi et al., 2016). Numerous studies have demonstrated correlations between RS data and various soil properties, with a notable focus on organic matter and particle size distribution. Regression analysis models are commonly employed for soil parameter prediction (da Silva Chagas et al., 2016, Nanni and Demattê, 2006, Stevens et al., 2010, Liao et al., 2013). GIS and regression analysis were employed to investigate the physical and chemical properties of the soil within Kirkuk city, establishing correlations among these properties (Sulyman et al., 2020, Raheem and Omar, 2021, Raheem et al., 2022). GIS was also utilized to determine the distribution of physical properties in Sulaimani, while a regression model was employed to predict physical properties in Egypt (Ahmed et al., 2022, Shahien and Ogila, 2022). The study of heavy, light, and clay minerals within formations is crucial due to their significance in various industries. In general, studies on the Injana and Fatha Formations have investigated their physical, chemical, and mineral properties. For instance, (Ismail and Omar, 2014) examined the physical and chemical properties of claystone in the Fatha Formation to assess its suitability as a raw material for clay brick manufacturing. Furthermore, the distribution of heavy, light, and clay minerals in Hindiya, Iraq, was determined through the use of RS and GIS, with Landsat images proving valuable in mineral distribution analysis (Saleh). The Injana and Fatha Formations in Kirkuk cover a vast area and encompass essential elements applicable to diverse industries, including brick production. However, due to the expansive coverage, comprehensive studies across all formations are challenging. Hence, the development of a model using GIS, RS, and regression analysis becomes imperative for predicting the physical and chemical properties of clay and minerals. This research aims to investigate the physical and chemical properties of the Injana and Fatha Formations and establish correlations among different elements by utilizing GIS, RS, and a regression analysis model.

2. Materials and Methods

2.1 Location and Geologic Setting of the Study Area

The selected area is located in the northern part of Iraq, which lies between the longitudes of 44° 10' E and 44° 40' E and latitudes 35° 10' N and 5° 40' N (Fig. 1). The selected area occupies ~268 Km^2. Its elevation ranges between 200 m and 400 m a.s.l. There are a number of important geological structures spread within the study area, such as the Kirkuk, Bor, Jambor, Fatha and Injana Formations within these structures. The climate of the region exhibits characteristics of a semiarid and Mediterranean climate. The primary period of precipitation typically spans from December to March.

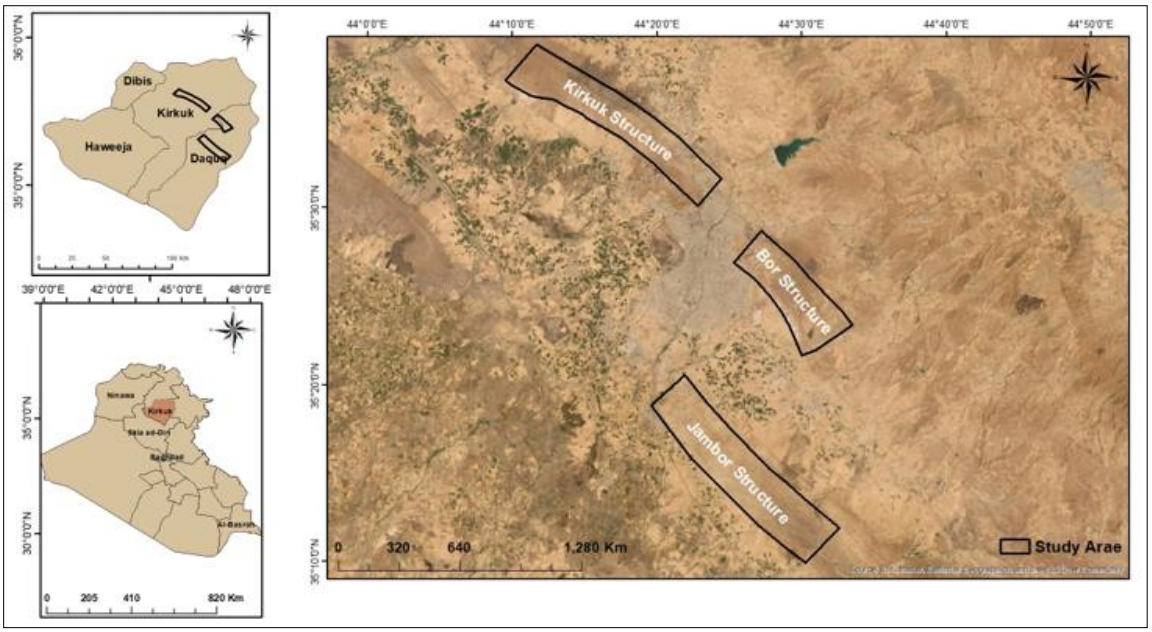


Fig. 1. Location map of the study area

2.2 Geology of the Study Area

The city of Kirkuk is situated in the hilly northern part of the Kirkuk Plain, approximately 340-360 meters above sea level. The Kirkuk structure, also known as the Baba Dome, and the Hamrin structure mark the northern and eastern boundaries of the plain, while the Hamrin structure and the lower Zap River outline the western and northern margins, respectively, as described by Buday (1980).

Significant tectonic movements occurred on Earth during the Pliocene period, resulting in the formation of several structures, including the Kirkuk, Bia-Hassan, Khabaze, Jambur, and Hamrin structures, as well as the Kirkuk-Hawija plain. The highest areas, which were composed of resistant rocks, experienced significant erosion, with the eroded materials being transported from higher ground and deposited in lower areas, as explained by the occurrence of a landslide (Jassim and Goff, 2006).

2.2.1. Fatha Formation

The lower Fars Formation, known as the Fatha Formation, is situated in northern Iraq, specifically 10 kilometers north of Baiji town, near the Makhul-Hamrin Range. This formation is primarily characterized by evaporitic deposits and comprises multiple cyclic sequences of mudrocks, limestones, gypsum, anhydrite, and halite (Fig. 2) (Jassim and Goff, 2006, Al-Juboury and McCann, 2008, Alhirmizy, 2015). The mudrocks within the Fatha Formation encompass marls, silty marls, and sandy marls, all of which are carbonate-rich (Al-Jaberi and Salim, 2022). These beds exhibit varying thicknesses ranging from 0.1 to 4.5 meters. Petrographically, the silty marl contains silt-sized quartz and feldspar grains embedded in a clayey and carbonate groundmass, typically displaying a red coloration. The marls consist of various minerals, including calcite, dolomite, quartz, feldspar, and clay. Clay minerals such as palygorskite, illite, kaolinite, and chlorite are also present (Al-Juboury and McCann, 2008, Al-Jaberi and Salim, 2022).

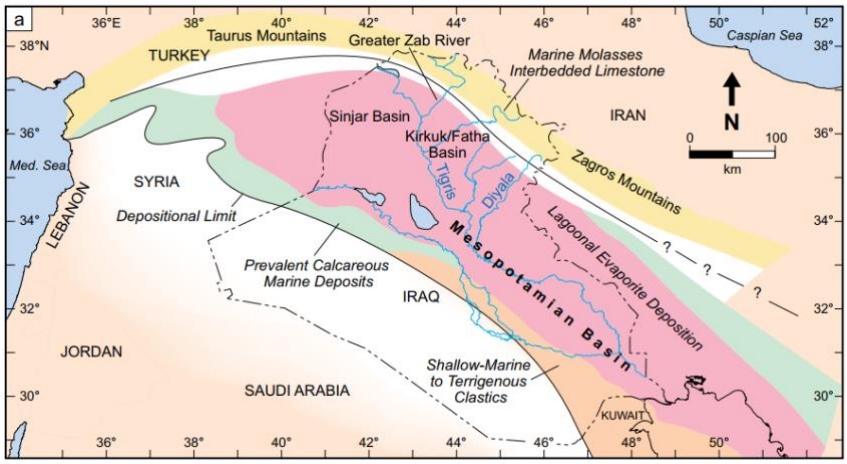


Fig. 2. Lithofacies distribution map of the Fatha Formation (Al-Juboury and McCann, 2008).

2.2.2. Injana Formation

According to (Jassim and Goff, 2006, Al-Juboury, 2009), the Injana formation has been proposed as a viable alternative to the Upper Fars formation in Iraq. This formation consists of several beds comprising sandstones, siltstones, and mudstones, as depicted in Fig.3. The thickness of these beds can vary from 1 to 15 meters, depending on sedimentary cycles. Located in the south Hamrin anticline near the Baghdad-Kirkuk road, the Injana Formation is widely distributed in Iraq, extending into northern Syria and Turkey and covering extensive areas of southern Iran (Alhirmizy, 2015, Obaid et al., 2022, Ali et al., 2023). The upper Miocene Injana Formation may be found throughout a major portion of Iraq. It also extends into northern Syria and Turkey, and it covers vast portions of southern Iran (Jassim and Goff, 2006, Al-Juboury, 2009). It is estimated that claystone constitutes a significant portion, ranging from 45% to 55%, of the overall sedimentary rock sequences (Awadh and Awad, 2020, Ali et al., 2023). The clay mineralogy of the mudstone units reveals the presence of illite, chlorite, palygorskite, and a mixture of illite-smectite layers (Al-Juboury, 2009).

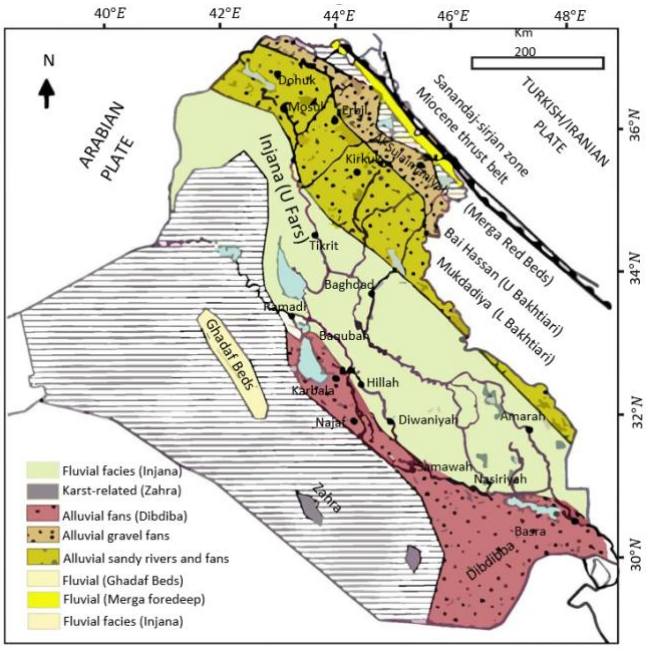


Fig. 3. Lithofacies distribution map of the Injana Formation (Jassim and Goff, 2006).

2.3. Field Measurements and Soil Analysis

In October 2022, a total of 52 topsoil samples were randomly collected from the Fatha and Injana Formations, covering an area of 268.12 km^2. These samples were distributed as follows: 13 samples from the Jambor structure, 20 samples from the Bor structure, and 19 samples from the Kirkuk structure. Each sample consisted of approximately 5 kilograms of soil, carefully labelled and placed in plastic bags for transportation to the laboratory. The coordinates of each sampling location were recorded using a global positioning system (GPS) device (Fig. 4).

In the laboratory, various tests were conducted to determine the basic properties of clay following standardized testing protocols. The dry density and water content of the samples were determined in the field using an HS-5001EZ moisture-density meter. The physical properties, including the Atterberg limits, specific gravity, and soil particle size, were determined using ASTM methods. The chemical properties were analysed in accordance with BS 1377-3, 1990 guidelines.

For further analysis, the samples underwent X-ray diffraction (XRF) major and trace element and X-ray diffraction (XRD) mineral identification analyses, which were carried out in a laboratory located in Turkey. These analyses provide valuable information on the elemental composition and mineralogical characteristics of the soil samples.

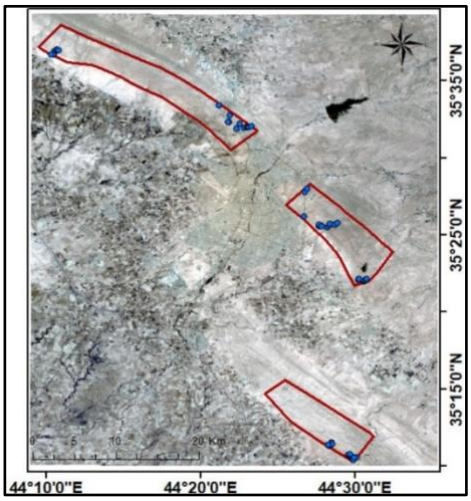


Fig. 4. The location of the point (a) Kirkuk structure; (b) Bor structure, and (c) Jambor structure

2.4. Physical Properties

The physical properties of soil encompass various characteristics, such as texture, dry density, specific gravity, Atterberg limits, and water content, all of which have significant implications for erosion, nutrient cycling, and biological activity. Understanding these properties is crucial for a range of industries.

Dry density (g/m^3), soil texture and moisture content are key factors in determining the maximum density achievable under consistent compaction energy (Goldsmith et al., 2001). Each textural composition of soil has a maximum attainable dry density at the optimal moisture level (Goldsmith et al., 2001). Moisture content (%) plays a vital role in the three-phase system of soil, which consists of minerals (solids), air, and moisture (SU et al., 2014),

Soil moisture exists in three forms: hygroscopic moisture, gravitational moisture, and capillary moisture. Determining the water content and dry density in the field is performed directly using a moisture-density meter such as the HS-5001EZ.

Specific gravity, the ratio of the unit weight of a material to the unit weight of water, is frequently required for various computations and can range from 2.6 to 2.9 for clayey and silty soils (Das and

Sivakugan, 2015). Particle size is used to classify soil into gravel, sand, silt, and clay categories based on the size of the predominant particles (Das and Sivakugan, 2015). This study specifically focuses on clay, which consists of tiny and submicroscopic particles of mica, clay minerals, and other minerals, typically less than 0.002 mm in size. Clays exhibit plasticity when combined with minimal water content (Das and Sivakugan, 2015). Particle size analysis of soil is typically performed using the hydrometer test.

The Atterberg limits describe the behavior of clayey soil when subjected to varying moisture levels. Excessive water content transforms the soil into a semiliquid state, and as it gradually dries, it transitions from plastic to semisolid or solid-states (Balasubramanian, 2017). The liquid limit (LL) is the moisture content at which the soil transitions from a liquid to plastic state, while the plastic limit (PL) represents the moisture content at which it changes from a plastic to semisolid state (Balasubramanian, 2017, Das and Sivakugan, 2015). The plasticity index (PI) is calculated as the difference between the LL and PL (Polidori, 2007). The Casagrande method is commonly used to determine the LL, while a soil thread with a diameter of 3 mm is employed to ascertain the PL.

2.5. Chemical Properties

Studying the chemical properties of soil provides valuable insights into its behavior and its potential applications in various industries. These properties encompass pH value, electrical conductivity (EC), organic matter content, gypsum content, total soluble salt (TDS) ratio, chloride concentration, and sulfate content. The pH value represents the logarithmic measure of hydrogen ion concentration, indicating the acidity or alkalinity of a solution (McLean, 1983, Sulyman et al., 2020). EC quantifies a material's ability to conduct electricity, often reflecting the movement of ions in the pore space of wet geomaterials (Klein and Santamarina, 2003, Sulyman et al., 2020). The organic matter content of the soil is influenced by factors such as composition, temperature, water distribution, and external conditions (Buee et al., 2007).

TDS refers to the salinity ratio in the soil, reflecting the proportion of dissolved salts. The solubility of salts can vary greatly depending on environmental factors such as temperature, pH, dissolved carbon dioxide (CO_2), evaporation rate, and moisture content (Ali et al., 2023). Sulfate is a chemical compound that occurs naturally and is readily accessible in various mineral forms. Its presence in the environment can be attributed to atmospheric and ground processes (Sulyman et al., 2020).

The pH measurement was conducted using a pH meter (PCTestr 35), while TDS and EC measurements were performed using a portable TDS and EC meter. The gypsum content was determined by subjecting the sample to a temperature of 150 °C, and the organic content was determined by burning the sample at 700 °C in an oven. Chloride concentrations were calculated using Mohr's method. These methods allowed for the quantification of the respective chemical properties of the soil samples.

2.6 . Major and Trace Elements

Metals exist naturally in the Earth's crust and are also present in the parent rocks that give rise to soil through the process of weathering. However, the distribution of metals varies across different geographic regions (Zovko and Romic, 2011). Heavy mineral analysis is one of the most sensitive and widely used techniques in the determination of sand and sandstone provenance (Mohammed et al., 2018). Heavy elements, known for their toxicity and long-lasting nature, are significant environmental pollutants due to their ability to be transported over long distances from their original sources (Ali et al., 2021). Human activities contribute significantly to the release of these elements into the environment, and they possess high chemical reactivity in environmental systems. Urban and industrial settings are potential sources of contamination, with heavy elements and other hazardous chemicals being released through processes such as industrial and transportation combustion. Manufacturing activities associated

with the extraction and production of industrial mineral products can also result in the discharge of substantial quantities of pollutants into the atmosphere, soil, and water (Zovko and Romic, 2011, Ali et al., 2021). In this study, the chemical elements were determined using XRF analysis conducted in a laboratory located in Turkey.

2.7. Clay Minerals

Clay minerals are vital components in agriculture and belong to a group of hydrous aluminum silicates known as phyllosilicates or layer silicates, characterized by their small particle size of less than 2 micrometers. Among the various types of clay minerals, five forms hold significant importance: chlorite, illite, vermiculite, montmorillonite-smectite, and kaolinite (Dogan, 2009). These clay minerals play a critical role in soil chemistry by influencing the flow and retention of contaminants, metals, and minerals. Furthermore, they exhibit excellent water and nutrient holding capacity, which is beneficial for moisture availability and nutrient availability for plants (Grim, 1962, Dogan, 2009).

2.8. XRD

XRD (X-ray diffraction) is a valuable technique used to identify minerals that are not easily identifiable through other means. It involves the generation of X-rays within an X-ray tube, which are then directed towards the sample. The diffracted X-rays are collected and recorded as the sample and detector rotate through their respective angles. This fundamental principle forms the basis of all diffraction techniques. During the process, when the mineral possesses lattice planes with sufficient d-spacing to diffract X-rays at a specific angle denoted as θ, the intensity of the diffracted X-rays reaches its maximum level (Brady et al., 1995, Ismail and Omar, 2014). XRD thus provides valuable information for the identification and characterization of minerals.

2.9. Remote Sensing

RS refers to the noncontact study of a subject by collecting and analysing data from a distance, without physical interaction (Lillesand et al., 2015). The Landsat satellite is widely regarded as one of the most effective in the field of RS (Scaramuzza et al., 2011, Shareef et al., 2018).

In this study, one of the main objectives is to utilize satellite image digital numbers (DNs) as parameters for predicting soil properties. To perform this prediction, the statistical package for the social sciences (SPSS) was used to apply the regression analysis. Given the time and cost constraints associated with traditional soil analysis methods, the integration of satellite imagery becomes crucial. To establish the correlation between DN values from the satellite bands and soil properties, we conducted soil sampling and analysis as outlined in the introduction. Subsequently, the analysis results were added to the database and integrated into ArcMap, where the sample site was georeferenced.

In our study, we used Landsat-8 and Landsat-7 ETM+ images. The image of Landsat-7 ETM+ that was taken after 2003 has duplicate scan lines. Therefore, we cannot use this image in any analysis because if we remove these scan lines and fill in the gaps, the images that are obtained after being corrected will not be similar to the original image (Dogan and Kılıç, 2013). (Dogan and Kılıç, 2013). Therefore, we used the Landsat image that was taken on 24 July 2001 (path/row: 169/035) that was downloaded free of cost for all bands from USGS-Earth Explorer. Landsat 8 was taken on 26 July 2022 (path/row: 169/035) and was downloaded free of cost for all bands from USGS-Earth Explorer in TIFF format. Subsequently, the images underwent georeferencing. A mosaic covering the entire research area was created in ArcMap. A region of interest (ROI) was selected to subset the satellite image, and radiometric enhancement techniques were applied to mitigate the effects of haze. Grid map layers of Landsat-7 ETM+ and Landsat-8 band DN values were created using the subset image in ArcMap.

The subsequent steps involved extracting the DN values from all bands and adding them to the database in ArcMap. In the regression analysis for predicting soil properties, the DN variables were treated as dependent variables, while the soil properties served as independent variables. Various regression techniques, including linear, multilinear, and nonlinear regressions, were employed to identify strong correlations and determine the Pearson correlation coefficient (R). The statistical analyses were conducted using SPSS software version 28. After that, significant relationships were used to map some soil properties in the study area. Using Landsat-7 and Landsat 8 bands and GIS map computation features, the resulting models were exported as grid map layers. Grid maps (DN values of bands) provide the basis for GIS map calculation functions, which include elementary mathematical operations such as addition, subtraction, multiplication, and division.

2.10. Regression analysis

Regression analysis is a fundamental statistical technique employed to estimate the value of a dependent variable based on independent variables and to ascertain the relationship between them (da Silva Chagas et al., 2016). There exist various types of regression models, including linear, multilinear, and nonlinear regressions. The fundamental equation used for regression analysis is as follows:

$$Y = a + b * X \quad \text{(Shareef et al., 2014)} \qquad (1)$$

To account for the nonlinear relationship between soil properties, we employed both multilinear and nonlinear regression techniques using the Statistical Package for the Social Sciences (SPSS) software. This approach allowed us to capture the complex associations between the various soil properties under investigation.

3. Results and Discussion

The soil samples underwent analysis to evaluate their physical and chemical properties, identify mineral compositions, and establish correlations between these properties and the satellite image data.

3.1. Field Measurement

Field measurements were conducted to determine the dry density and water content, yielding the following results:

Dry density: Ranged from 1.185 to 2.112 g/m^3. Notably, the dry density within the Fatha Formation was lower than the dry density within the Injana Formation. Water content: Ranged from 2% to 20%.

3.2. Physical Properties

The analysis of particle sizes in the fifty-two soil samples uncovered noteworthy findings. Silt was found to dominate the majority of samples, varying from 28% to 93%. Conversely, gravel constituted the smallest proportion in most samples, with percentages ranging from 0% to 4%, except for one site where it reached 16%. The sand content was generally low, ranging from 0% to 30%. However, two locations exhibited unusually high sand percentages of 42% and 61%. The clay content ranged from 1% to 38%, with the highest clay concentration observed in the Injana Formation within the Kirkuk structure.

Moreover, the Atterberg limits analysis provided additional insights. The LL, which measures the moisture content at which soil transitions from a plastic to a liquid state, varied from 18% to 43%, with an average of 30%. The PL, which represents the moisture content at which soil starts exhibiting plastic behavior, ranged from 16% to 22%, averaging 19%. The PI, defined as the difference between the liquid

limit and plastic limit, displayed values ranging from 2% to 21%. The majority of the samples exhibited a plasticity index between 5% and 20%, indicating a range of low to medium plasticity.

3.3. Chemical Properties

The chemical analysis of soil properties in the study area revealed the following ranges and averages:
Organic matter: Ranged from 3.4% to 6.7%
Chloride: Ranged from 0.01% to 5%, with an average of 0.02%
pH: Ranged from 6.7 to 7.5%
Gypsum: Ranged from 2.5% to 7%, except for two locations in the Fatha Formation with high ratios of 19% and 41%
Sulfate: Ranged from 1.2% to 3.3%, except for two locations in the Fatha Formation with ratios of 8.8% and 19%. The percentage of sulfur in the study area was higher compared to a previous study conducted in 2007, where the range was from 0% to 3% (Maala et al., 2007). This lower sulfur content can be attributed to its scarcity in gypsum, anhydrite, and claystone.
T.D.S.: Ranged from 2 to 18.8.
It is worth noting that the primary gypsum deposits in Iraq are predominantly found in the middle Miocene Fatha Formation. Within this formation, more than ten thick gypsum layers alternate with claystone and limestone, as documented by (Al-Bassam, 2012).

3.4. Regression Analysis

Once all the results have been integrated into the database, the correlation between parameters is examined using SPSS software through regression analysis. This model enables the assessment of relationships and correlations among the variables in the dataset.

3.4.1. Linear Regression between the Chemical Properties

The linear correlation analysis, presented in Table 1, reveals that there is no linear regression between organic matter and other chemical properties. However, chloride demonstrates a weak positive correlation with the pH value and a strong positive correlation with EC and TDS, with correlation coefficients of 0.686 and 0.702, respectively.

Moreover, gypsum and sulfate exhibit a weak positive correlation with the pH value, EC, and TDS. Additionally, the pH value demonstrates a moderately positive correlation with EC and TDS. Notably, a very strong correlation is observed, with a correlation coefficient of 0.99, between EC and TDS, as well as between gypsum and sulfate. (Fig. 5) show the Linear regression of chemical properties.

Table 1. Linear regression of chemical properties

Chnical Properties	Organic matter	Chloride	PH	EC	TDS	Gypsum	Sulfate
Organic matter	1						
Chloride	0.047	1					
PH	0.023	0.127	1				
EC	0.013	0.702	0.506	1			
TDS	0.012	0.686	0.517	0.99	1		
Gypsum	0.033	0.001	0.217	0.153	0.158	1	
Sulfate	0.033	0.001	0.217	0.153	0.158	0.99	1

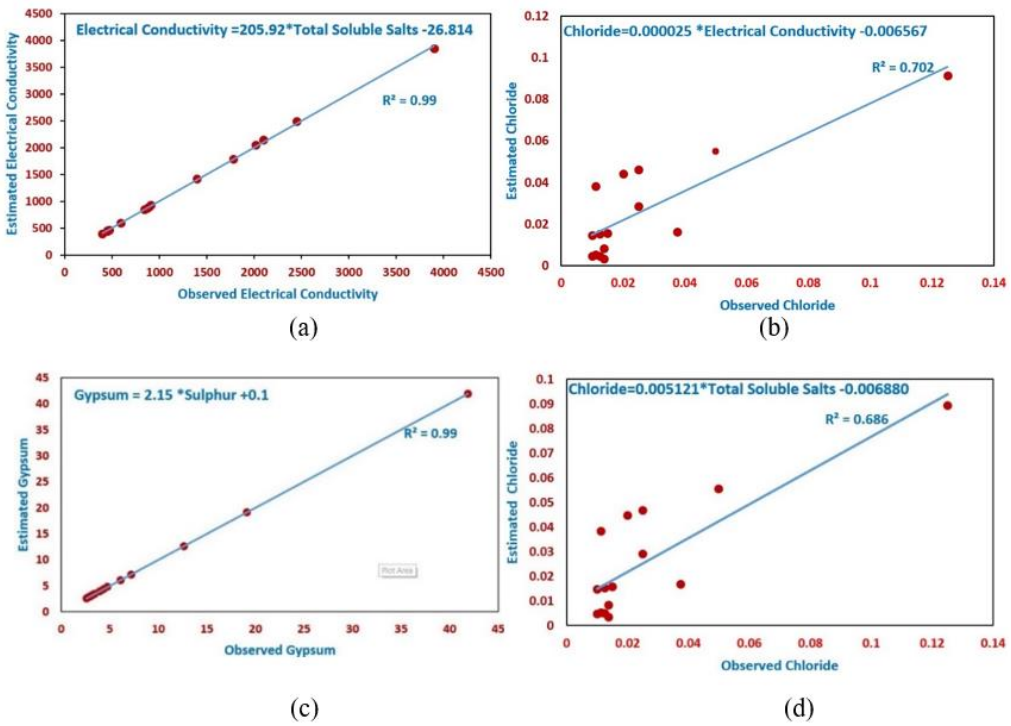


Fig. 5. Regression between chemical properties: (a) Regression between observed and estimated EC (using TDS as an independent variable); (b) Regression between observed and estimated chloride (using EC as an independent variable); (c) Regression between observed and estimated gypsum (using sulfate as an independent variable); (d) Regression between observed and estimated chloride (using TDS as an independent variable).

3.4.2. Linear Regression between the Chemical and Physical Properties

As part of this investigation, a regression analysis was performed to explore the relationship between physical and chemical properties and determine the most suitable equations for predicting soil properties. The outcomes, outlined in Table 2, indicate that weak or nonlinear correlations exist between these properties. Specifically, the highest correlation coefficients observed were 0.341 between the pH value and the plasticity index and 0.369 between the pH value and the LL. Fig. 6 shows the regression between chemical and physical properties.

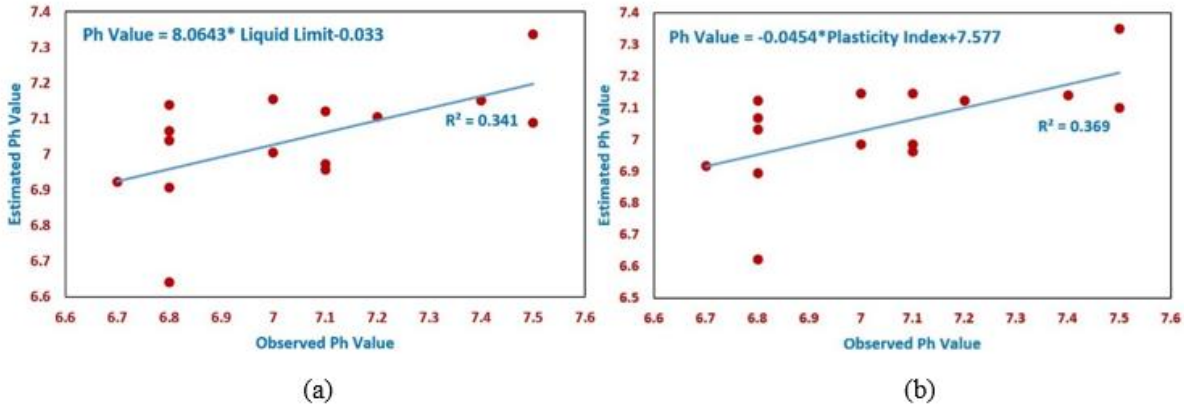


Fig 6. Regression between chemical and physical properties: (a) Regression between observed and estimated pH values (using LL as an independent variable); (b) Regression between observed and estimated pH values (using plasticity index as an independent variable).

Table 2. Linear regression of chemical and physical properties

	Water content	Dry density	Liquid Limit	Plastic Limit	Plasticity Index	Specific Gravity	gravel	Sand	silt	Clay
TDS	0.02	0.039	0.016	0.005	0.021	0.001	0.119	0.051	0.023	0.006
Organic Matter	0.281	0.055	0.126	0.182	0.107	0.033	0.021	0.23	0.034	0.089
Chloride	0.07	0.074	0	0	0	0.001	0.108	0.075	0.115	0.011
pH	0.044	0.02	0.341	0.242	0.369	0.084	0	0.045	0.05	0.264
EC	0.021	0.04	0.016	0.004	0.021	0.001	0.118	0.051	0.024	0.006
Gypsum	0.013	0.019	0.067	0.05	0.071	0.009	0.069	0.013	0.04	0.158
Sulfate	0.013	0.019	0.067	0.05	0.071	0.009	0.069	0.013	0.04	0.158

3.4.3. Multiple linear regression between the chemical and physical properties

Multiple linear regression is a predictive model utilized to estimate outcomes based on the association between multiple independent variables and a dependent variable. In this particular investigation, the multiple linear regression analysis revealed positive moderate correlations ranging from 0.604 to 0.72 between properties. These findings are visually represented in (Fig.7.) and are further detailed in Table 3.

Table 3. Multiple linear regression of chemical and physical properties

Equation	R^2
LL = 0.131 *Gravel + 0.005 * Sand + 0.597 * Clay + 23.61	0.704
LL = 1.18 * Organic Matter + 154 * Chloride -23 * pH – 0.008 * EC +0.3 * sulfate+ 193	0.711
PL = -0.024 * Sand – 0.027 * Silt + 0.122 * Clay + 20.06	0.604
PI = -0.101 * Sand – 0.104 * Silt + 0.345 * Clay + 16.64	0.720
Clay Content = 1.986 * LL – 3.103 * PL + 9.76	0.717

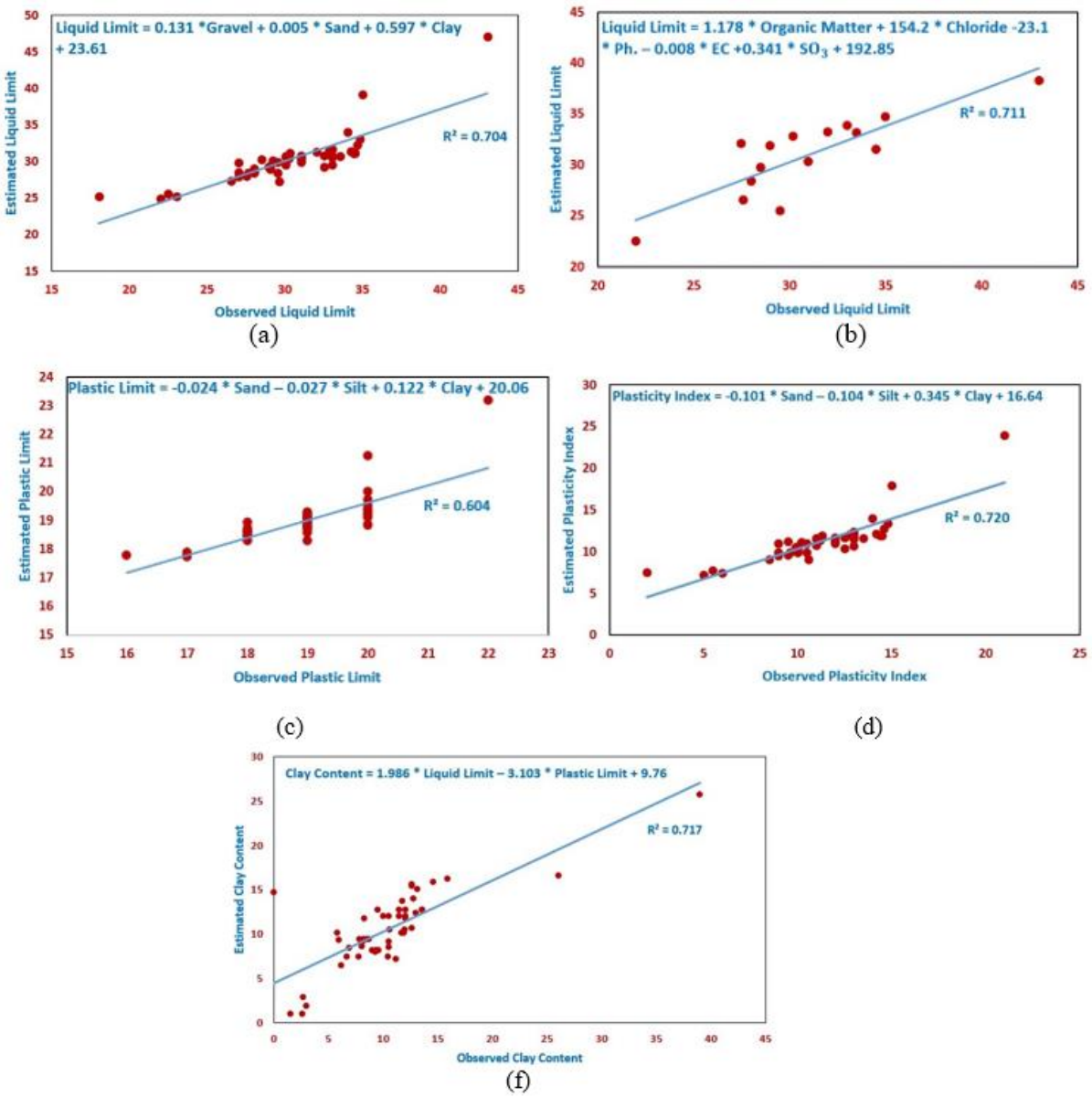


Fig 7. Multiple regression between chemical and physical properties: (a) Regression between observed and estimated LL (using particle size as independent variable); (b) Regression between observed and estimated LL (using chemical properties as independent variable); (c) Regression between observed and estimated PL (using particle size as independent variable); (d) Regression between observed and estimated PI (using particle size as independent variable); (f) Regression between observed and estimated clay content (using Atterberg limit as independent variable).

3.4.4. Nonlinear regression between the chemical and physical properties

Nonlinear regression is a regression analysis method that involves fitting data to a model expressed as a mathematical function. Unlike linear regression, which assumes a linear relationship between variables, nonlinear regression allows for curved relationships between the variables.

Given the weak strength of the linear regression observed between the properties, nonlinear regression was employed to establish a more robust correlation with higher correlation coefficients. The outcomes of the nonlinear regression analysis are presented in Tables 4, 5, 6, and 7.

The results of the nonlinear regression model demonstrate improved correlations between the parameters compared to linear regression. In many cases, the relationships were best described by cubic and quadratic equations, indicating the presence of nonlinearity in the data. By utilizing nonlinear regression, a more accurate estimation of the relationships between variables was achieved.

Table 4. Nonlinear regression of chemical properties

Chnical Properties	**Organic matter**	**Chloride**	**PH**	**EC**	**TDS**	**Gypsum**	**Sulfate**
Organic matter	1						
Chloride	0.005	1					
PH	0.246	0.173	1				
EC	0.1	0.925	0.823	1			
TDS	0.098	0.928	0.819	1	1		
Gypsum	0.049	0.28	0.543	0.646	0.658	1	
Sulfate	0.049	0.28	0.543	0.646	0.658	1	1

Table 5. Nonlinear regression of physical properties

	Water content	**Dry density**	**LL**	**PL**	**PI**	**Specific Gravity**	**Gravel**	**Sand**	**Silt**	**Clay**
Water content	1									
Dry density	0.07	1								
LL	0.153	0.091	1							
PL	0.176	0.095	0.94	1						
PI	0.14	0.083	0.992	0.895	1					
Specific Gravity	0.161	0.2	0.113	0.084	0.121	1				
Gravel	0.058	0.019	0.039	0.028	0.042	0.937	1			
Sand	0.033	0.006	0.114	0.138	0.104	0.417	0.558	1		
Silt	0.004	0.023	0.067	0.08	0.063	0.315	0.553	0.823	1	
Clay	0.157	0.082	0.818	0.74	0.823	0.061	0.074	0.155	0.097	1

Table 6. Nonlinear regression of physical and chemical properties

	Water Content	Dry Density	LL	PL	PI	Specific Gravity	gravel	Sand	silt	Clay
TDS	0.382	0.061	0.197	0.157	0.207	0.393	0.206	0.061	0.126	0.2
Organic Matter	0.308	0.189	0.216	0.229	0.258	0.325	0.074	0.396	0.111	0.354
Chloride	0.116	0.116	0.007	0.008	0.009	0.054	0.207	0.127	0.201	0.085
pH	0.323	0.232	0.37	0.25	0.42	0.197	0	0.05	0.062	0.409
EC	0.385	0.062	0.199	0.158	0.209	0.392	0.202	0.06	0.12	0.21
Gypsum	0.048	0.023	0.105	0.071	0.132	0.047	0.146	0.138	0.19	0.228
Sulfate	0.048	0.023	0.105	0.071	0.132	0.047	0.146	0.138	0.19	0.228

Table 7. Nonlinear regression of physical and chemical properties

Equation	Parameters				R^2
	b0	b1	b2	b3	
LL=b0 +(b1*PI)+(b2*PI^2)+ (b3*PI^3)	15.525	1.188	0.017	-0.001	0.992
PI=b0 +(b1*LL)+(b2*LL^2)	-10.383	0.686	0.001	0	0.992
LL=b0+(b1*Clay)+(b2*$Clay^2$)+(b3* $Clay^3$)	17.559	1.889	-0.071	-0.001	0.818
Clay=b0 +(b1*LL)+(b2*LL^2)+)+(b3*LL^3)	-63.005	7.099	-0.261	0.004	0.843
PL=b0 +(b1*PI)+(b2*PI^2)+)+(b3* PI^3)	15.525	0.188	0.017	-0.001	0.895
PI=b0 +(b1*PL)+(b2*PL^2)	-23.702	1.024	0.043	0	0.895
PL=b0 +(b1*Clay)+(b2*$Clay^2$+(b3* $Clay^3$)	15.64	0.513	-0.02	-0.001	0.74
lnClay=b0+(b1/PL)	10.071	-148.069	0	0	0.723
PI=b0 +(b1*Clay)+(b2*$Clay^2$)+ (b3* $Clay^3$)	1.919	1.376	-0.051	-0.001	0.823
Specific gravity =b0+(b1*Gravel)+(b2*$Gravel^2$) +(b3*$Gravel^3$)	2.722	-0.065	0.028	-0.002	0.937
Gravel =b0 +(b1*Sand)+(b2*$Sand^2$)+ (b3* $Sand^3$)	0.661	-0.350	0.027	0.0001	0.558
Sand =b0 +(b1*Silt)+(b2*$Silt^2$)+ (b3* $Silt^3$)	136.333	-3.998	0.05	0.0001	0.823
Chloride =b0 +(b1*EC)+(b2*EC^2)+ (b3* EC^3)	0.007	1.718	-1.125	3.756	0.925
Chloride =b0 +(b1*TDS)+(b2*TDS^2)+ (b3* TDS^3)	0.005	0.005	-0.001	3.882	0.928
pH =b0 +(b1/EC)	6.653	318.93	0	0	0.823
pH =b0 +(b1/TDS)	6.651	1.604	0	0	0.819
pH =b0 +(b1*Gypsum)+(b2*$Gypsum^2$)+ (b3* $Gypsum^3$)	7.687	-0.188	-0.01	0.0001	0.543
TDS =b0 +(b1*Gypsum)+(b2*$Gypsum^2$)+ (b3* $Gypsum^3$)	-6.957	3.975	-0.22	0.003	0.658

The results of the nonlinear regression model show that the correlation between the parameters is better than that of the linear regression; most of the nonlinear relationships were expressed by cubic and quadratic equations.

3.4.5. Major and trace elements

The results of XRF analysis are presented in Tables 8 and 9, showcasing the values of essential major and trace elements. The percentage of SiO_2 was found to be high in all samples, ranging from 26.5% to 49.69%. Moreover, the SiO_2 content in the Fatha Formation exceeded that in the Injana Formation. This finding aligns closely with previous studies conducted in 2005 and 2007, which reported SiO2 percentages ranging from 24.7% to 58.5% in the Fatha Formation (Jobouri, 2005, Maala et al., 2007). Felspar, quartz, and other heavy minerals are recognized as primary sources of silica (Hussein et al., 2021). The MgO content ranged from 4.224% to 8.868%, while CaO exhibited high values in all samples, ranging from 11.85% to 23.95%. The presence of CaO is crucial in defining the limits of sand cements, as indicated by (Farquhar et al., 2015). Specifically, sediments are classified as noncalcareous if CaO < 4%, calcareous if 4% < CaO < 15%, and carbonate if CaO > 15%. Thus, the studied sediments can be classified as carbonate, with the lowest percentage observed in the Fatha Formation. Sodium oxide (Na_2O), phosphorus pentoxide (P_2O_5), titanium dioxide (TiO_2), chromium trioxide (Cr_2O_3), and manganese oxide (MnO) were present in all samples, albeit in relatively low percentages.

The analysis of trace elements revealed that cobalt (Co) ranged from 40.7 to 68.5 ppm. Nickel (Ni) exhibited values ranging from 103 to 308 ppm, surpassing the Ni values reported in a study by (Ali et al., 2021). Additionally, the average copper (Cu) content was determined to be 24.4 ppm, which is

lower than the Cu concentration reported in the Al-HAWIJA study (39.53 ppm) conducted by (Al-Obeidi and Al-Jumaily, 2020).

Table 8. Major Elements

Element	A3	A7	d1	d2	d3	d4	d6	P1	P2	P3	P9	P13
Na_2O	0.055	0.046	0.913	0.9364	1.0468	0.048	0.048	0.4772	0.8935	0.6837	0.046	0.047
MgO	4.224	7.237	7.188	8.8683	6.9142	7.82	9.093	5.1678	5.5028	5.4353	5.077	3.709
Al_2O_3	12.02	11.556	13.01	12.379	10.802	11.025	12.8	10.29	13.42	13.913	14.89	14.16
SiO_2	44.35	36.42	29.44	28.8	27.93	42.87	49.69	26.5	29.66	28.77	47.93	45.82
P_2O_5	0.1936	0.1639	0.169	0.1632	0.1971	0.1822	0.1795	0.1785	0.182	0.1803	0.1934	0.175
SO_3	1.712	3.309	0.652	0.9141	5.1835	0.1154	2.229	3.4226	0.648	1.3502	0.1196	0.109
K_2O	2.141	2.06	1.462	1.4961	1.2318	1.569	2.633	1.3343	1.6272	1.6033	2.515	2.428
CaO	18.22	19.34	20.89	22.32	22.08	20.68	11.851	23.95	19.26	20.78	18.45	19.67
TiO_2	0.6265	0.5351	1.239	1.1689	1.0184	0.6386	0.636	0.9619	1.2531	1.1834	0.7156	0.6242
Cr_2O_3	0.0271	0.0439	0.135	0.1306	0.078	0.0633	0.0202	0.0728	0.0644	0.0647	0.0213	0.0178
MnO	0.0948	0.0766	0.216	0.2612	0.1829	0.1121	0.157	0.2103	0.2183	0.2296	0.088	0.1034
Fe_2O_3	5.814	6.584	7.439	7.433	6.859	6.314	7.318	7.482	8.351	8.219	6.683	5.553

Table 9. Trace Elements

Element	Oran	A-3	A7	P13	P9	d4	d6
Co	ppm	68.5	58.4	54.1	60	51.5	40.7
Ni	ppm	144.7	308.6	103.4	138.8	273	146.4
Cu	ppm	32.1	17.4	19.8	32.6	23.4	21.3
Zn	ppm	78.8	76	79.3	92.6	76.9	87.6
Ga	ppm	14.1	13	16.1	15.7	11.3	16.4
Ge	ppm	1.4	1.5	0.6	1.7	0.9	0.4
As	ppm	9.6	3.1	6.2	8.9	5.9	8.2
Se	ppm	0.3	0.3	0.3	0.3	0.3	0.3
Br	ppm	2	0.3	0.3	0.8	0.8	1.1
Rb	ppm	76	57.4	85.6	90.7	47.8	90
Sr	ppm	325.7	191.4	301.3	270.6	355	331.6
Y	ppm	20.1	14.3	17.5	21.8	17.6	19.9
Zr	ppm	133.9	82.9	115.8	128.9	105.6	120.6
Nb	ppm	12.8	8.8	3.6	11.2	7.9	11.7
Mo	ppm	3.1	3.1	6.9	6.8	3.4	8.8
Cd	ppm	0.03	0.05	0.05	0.03	0.025	0.022
In	ppm	0.8	0.8	0.8	0.9	0.8	0.8
Sn	ppm	1.1	0.9	1	1	0.9	1.7
Sb	ppm	0.9	0.9	0.9	1.5	1.6	0.8
Te	ppm	1.2	1.1	1.2	1.2	1.2	1.1
I	ppm	2.4	6.8	2.3	2.9	2.1	2
Cs	ppm	3.6	3.5	3.7	6.9	3.5	3.5
Ba	ppm	257.8	121.9	358.7	259.1	257.3	285.9
La	ppm	28.4	17	20.2	28.2	18.2	29.5
Ce	ppm	47.6	25.5	33.3	43.3	23.9	55.4
Hf	ppm	3.4	2.8	2.7	3.1	3.1	2.8
Ta	ppm	3.9	3.9	3.1	3.9	4	3.6
W	ppm	3.1	4	3.1	3.3	3.8	3.3
Hg	ppm	0.0004	0.0002	0.0002	0.0001	0.0004	0.0001
Tl	ppm	0.9	0.9	0.9	0.9	0.8	0.9
Pb	ppm	13.2	1.9	11.5	13.4	13.4	14.8
Bi	ppm	0.6	0.6	0.6	0.6	0.6	0.6
Th	ppm	6.5	1	8.1	6.6	2.2	6.1
U	ppm	1.1	1.4	1.7	1.2	1.7	0.3

3.5. XRD

The results of XRD analysis for six samples from the Fatha and Injana Formations are depicted in Fig. 8 and 9. In the Injana Formation, nonclay minerals identified include quartz, feldspar, K-feldspar, calcite, and muscovite-calcite. On the other hand, the nonclay minerals present in the Fatha Formation consist of quartz, feldspar, K-feldspar, calcite, calcite-dolomite, and gypsum-calcite.

The clay component in both the Injana and Fatha Formations primarily comprises calcite, which is blended with carbonate in sandstone. Quartz was observed as a widespread mineral in the clay samples. In most samples, the quantity of quartz exceeded that of calcite, except in one sample from the

Fatha Formation, where calcite outweighed quartz. Feldspar was found to be present in low concentrations across all samples.

The clay minerals identified in the Injana Formation include chlorites-montmorillonite, illite, chlorites, illite-palygorskite, palygorskite, illite-muscovite, and gypsum. In the Fatha Formation, the clay minerals consist of chlorites-montmorillonite, illite, chlorites, gypsum, and palygorskite. The proportion of gypsum was higher in the Fatha Formation than in the Injana Formation due to the presence of gypsum in claystone and limestone within the Fatha Formation. Chlorites exhibited higher concentrations in the Injana Formation than in the Fatha Formation. Illite was found to be present in relatively low percentages across all samples.

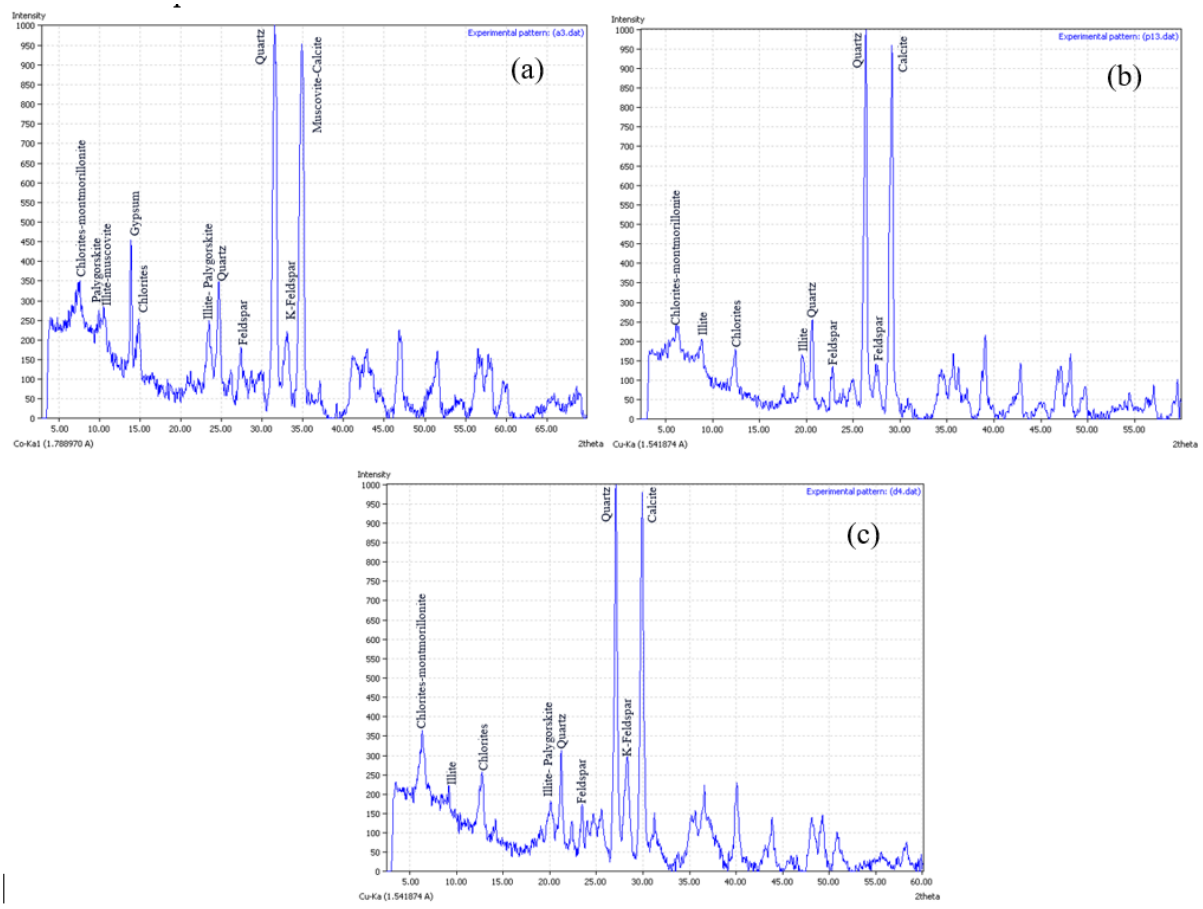


Fig. 8. The X-ray diffraction of the Injana formation: (a) XRD of sample (a3); (b) XRD of sample (p13); (c) XRD of sample (d4).

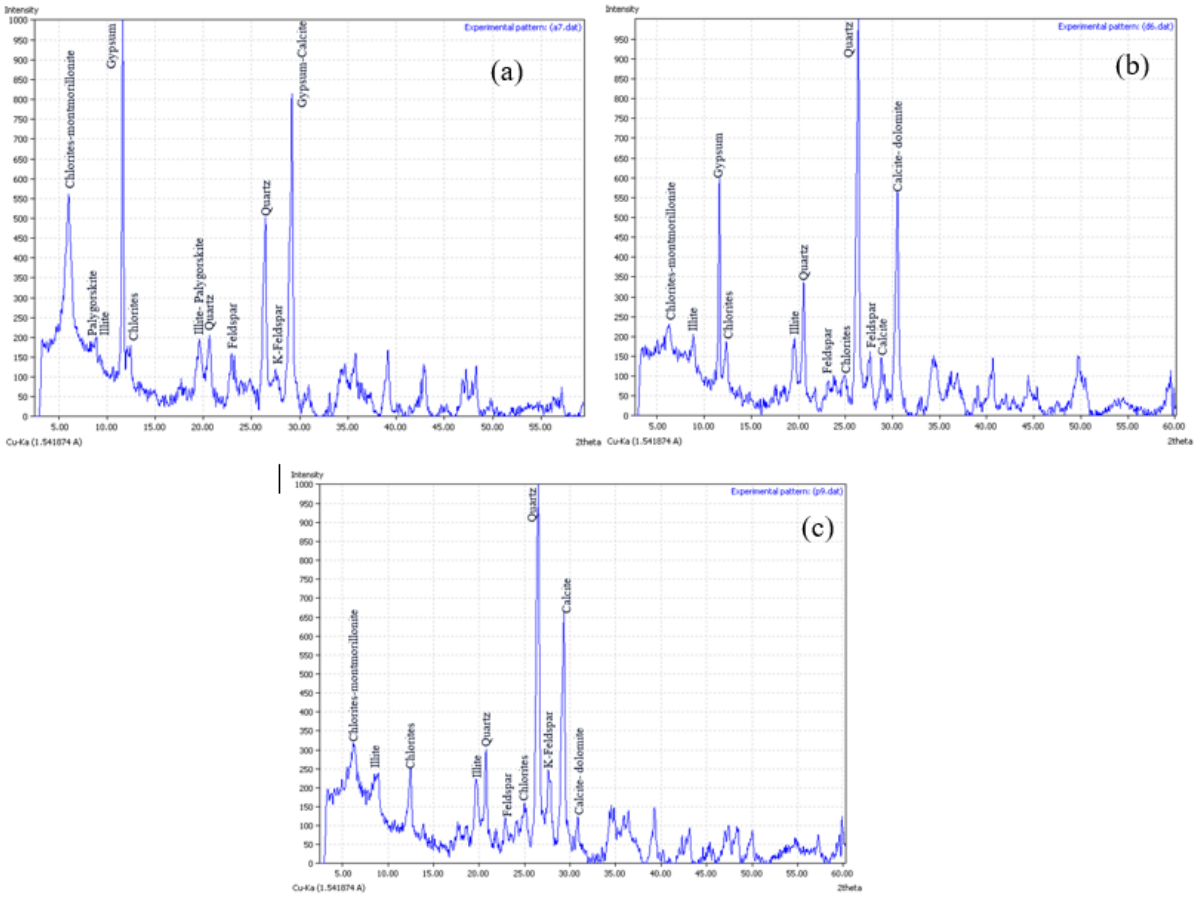


Fig 9. The X-ray diffraction of the Fatha Formation: (a) XRD of sample (a7); (b) XRD of sample (d6); (c) XRD of sample (p9).

3.6. RS

Landsat images serve as a valuable tool for acquiring data in challenging and inaccessible areas, particularly in remote or expansive regions. Given the wide study area with diverse topography, the characteristics of red clay were examined in relation to DN extracted from Landsat 7 and Landsat 8 images. The results, presented in Tables 10-13, highlight the correlation between physical and chemical properties with specific bands. The results show that the physical properties are correlated with the bands of Landsat 8. Chemical properties such gypsum and chloride have a correlation with band 3 in Landsat 7. The liquid limit, plastic limit, clay content, and chloride grid maps generated from the developed models were categorized using the natural breaks technique in the ArcMap program. The classes within each simulated soil variable were categorized into five distinct groups, as shown in Fig. 10 to Fig. 21.

When considering the correlation of physical properties with Landsat 7, it was observed that water content, dry density, specific gravity, and sand exhibited weak correlations, with correlation coefficients ranging from 0.044 to 0.162. However, silt and clay demonstrated a moderately positive correlation with band 1. In terms of chemical properties, except for gypsum, which showed a strong positive correlation with band 3, the remaining chemical properties displayed weak correlations.

Similarly, the correlation analysis of physical properties with Landsat 8 revealed weak correlations with water content, dry density, specific gravity, and sand, with correlation coefficients ranging from 0.048 to 0.232. Notably, silt, gravel, LL, and PL exhibited moderately positive correlations with bands 1 and 7. The clay content, on the other hand, displayed a strong positive correlation with band 1, with a $R^2$of 0.856. It is worth mentioning that this coefficient is higher than that reported in a previous study

(Hosseini et al., 2014), which reported a R^2 of 0.67. Furthermore, the chemical properties demonstrated moderately positive correlations with T.D.S., chloride, and EC.

Table 10. Nonlinear regression of physical properties and Landsat 7 data.

Landsat 7	Water Content	Dry Density	LL	PL	PI	Specific Gravity	gravel	sand	silt	Clay
B1	0.104	0.072	0.25	0.248	0.247	0.162	0.263	0.044	0.447	0.492
B2	0.089	0.09	0.181	0.171	0.183	0.088	0.252	0.022	0.345	0.473
B3	0.031	0.008	0.069	0.056	0.073	0.051	0.226	0.028	0.277	0.257
B4	0.041	0.036	0.107	0.088	0.111	0.092	0.217	0.042	0.247	0.271
B5	0.011	0.009	0.089	0.085	0.09	0.031	0.046	0.017	0.202	0.226
B7	0.052	0.007	0.069	0.079	0.064	0.026	0.005	0.212	0.153	0.102

Table 11. Nonlinear regression of chemical properties and Landsat 7.

Landsat7	T DS	Organic Matter	Chloride	pH	EC	Gypsum	Sulfate
B1	0.117	0.045	0.165	0.079	0.119	0.739	0.739
B2	0.187	0.032	0.237	0.091	0.187	0.721	0.721
B3	0.143	0.082	0.204	0.117	0.143	0.749	0.749
B4	0.077	0.077	0.233	0.107	0.077	0.723	0.723
B5	0.03	0.119	0.146	0.088	0.03	0.732	0.732
B7	0.03	0.296	0.071	0.054	0.03	0.423	0.423

Table 12. Nonlinear regression of physical properties and Landsat 8 data

Landsat 8	Water Content	Dry Density	LL	PL	PI	Specific Gravity	Gravel	Sand	Silt	Clay
B1	0.06	0	0.659	0.607	0.66	0.232	0.323	0.007	0.528	0.856
B2	0.101	0.031	0.576	0.486	0.593	0.188	0.223	0.012	0.495	0.84
B3	0.12	0.058	0.478	0.381	0.501	0.166	0.266	0.048	0.471	0.798
B4	0.047	0.02	0.542	0.454	0.559	0.179	0.308	0.013	0.533	0.793
B5	0.028	0.073	0.547	0.49	0.552	0.181	0.312	0.031	0.532	0.751
B6	0.039	0.049	0.562	0.538	0.557	0.198	0.252	0.018	0.498	0.756
B7	0.032	0.023	0.462	0.44	0.458	0.151	0.501	0.001	0.415	0.558

Table 13. Nonlinear regression of chemical properties and Landsat 8.

Landsat 8	TDS	Organic Matter	Chloride	pH	EC	Gypsum	Sulfate
B1	0.077	0.056	0.267	0.232	0.077	0.126	0.126
B2	0.252	0.055	0.323	0.312	0.252	0.272	0.272
B3	0.452	0.038	0.505	0.325	0.452	0.35	0.35
B4	0.374	0.029	0.454	0.36	0.374	0.194	0.194
B5	0.158	0.019	0.376	0.218	0.158	0.214	0.214
B6	0.035	0.005	0.253	0.103	0.035	0.214	0.214

Table 14. Nonlinear regression of physical and chemical properties with Landsat 7 and 8

Equation	Parameters			R^2
	b0	b1	b2	

LL=b0 +(b1*band 1)+(b2*band 1^2)	1500	-0.263	1.178	0.659
PL=b0 +(b1*band 1)+(b2*band 1^2)	380.559	-0.065	2.892	0.607
PI=b0 +(b1*band 1)+(b2*band 1^2)	1120.3	-0.199	8.889	0.660
Clay=b0 +(b1*band 1)+(b2*band 1^2)	2261	-0.410	1.861	0.856
Gravel=b0 +(b1*band 7)+(b2*band 7^2)	48.793	-0.005	1.390	0.501
Silt=b0 +(b1*band 5)+(b2*band 5^2)	-975.477	0.115	-3.116	0.532
Chloride=b0 +(b1*band 3)+(b2*band 3^2)	4.603	-0.001	1.989	0.505
Gypsum=b0 +(b1*band 3)+(b2*band 3^2)	981.769	-0.113	3.264	0.749

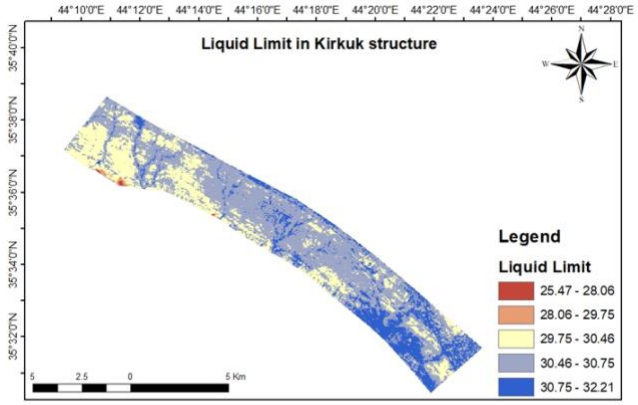


Fig. 10. Gird maps of liquid limit in Kirkuk structure (using classification: Natural Breaks, 5 classes)

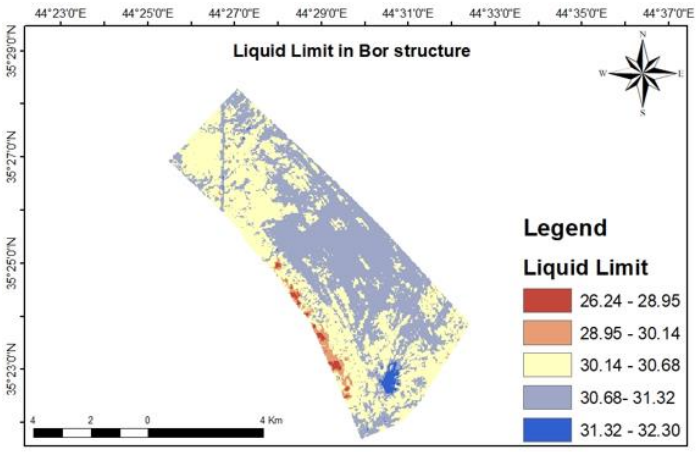


Fig. 11. Gird maps of liquid limit in Bor structure (using classification: Natural Breaks, 5 classes)

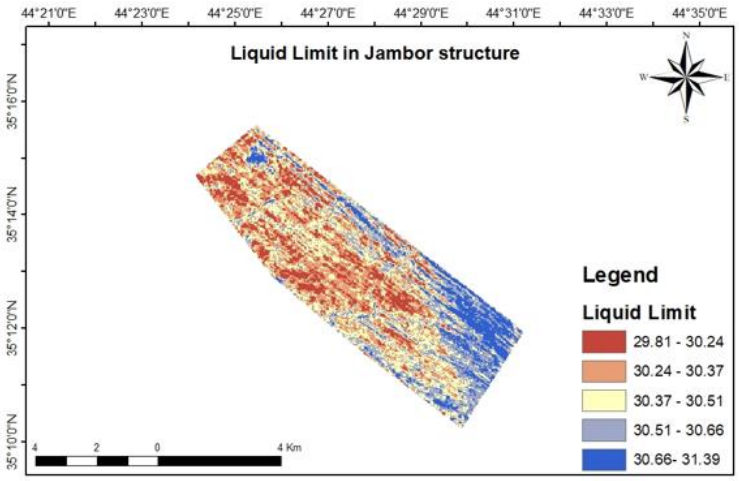


Fig. 12. Gird maps of liquid limit in Jambor structure (using classification: Natural Breaks, 5 classes)

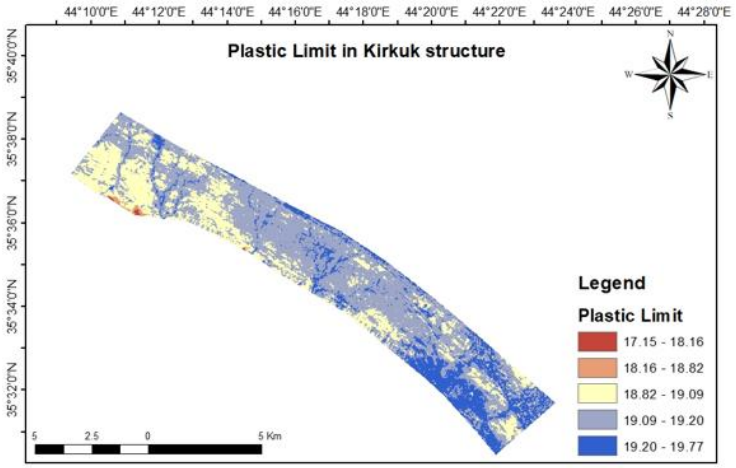


Fig. 13. Gird maps of plastic limit in Kirkuk structure (using classification: Natural Breaks, 5 classes)

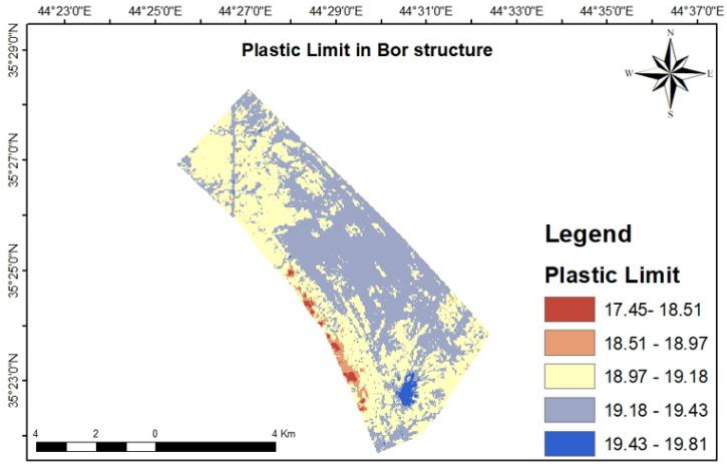


Fig. 14. Gird maps of plastic limit in Bor structure (using classification: Natural Breaks, 5 classes)

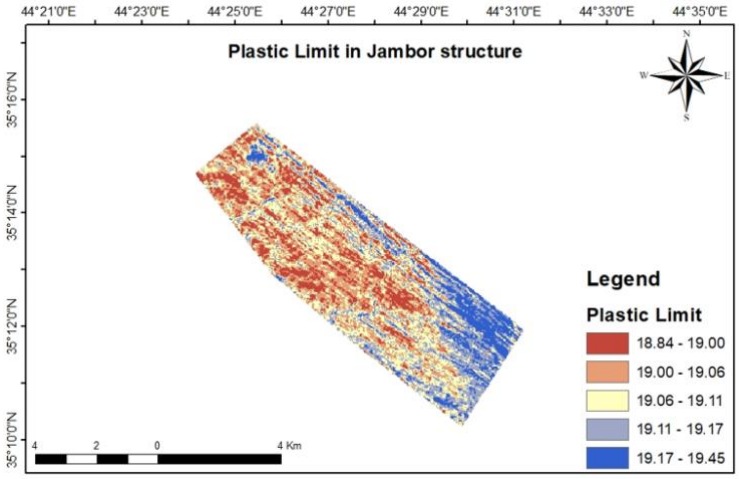


Fig. 15. Gird maps of plastic limit in Jambor structure (using classification: Natural Breaks, 5 classes)

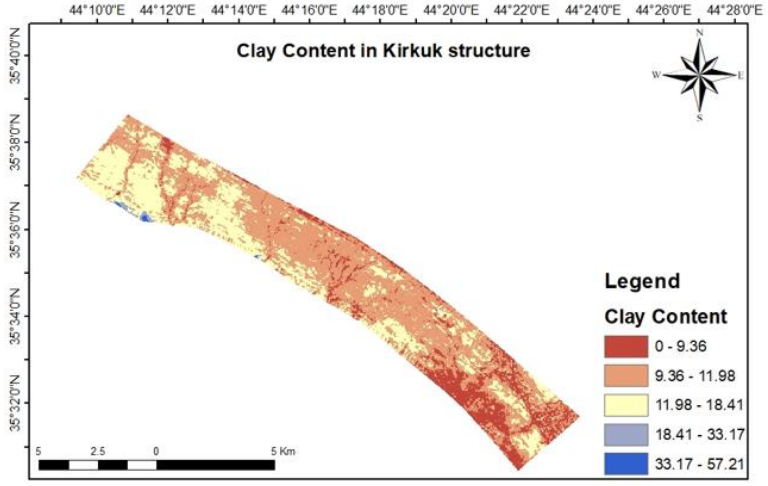


Fig. 16. Gird maps of clay content in Kirkuk structure (using classification: Natural Breaks, 5 classes)

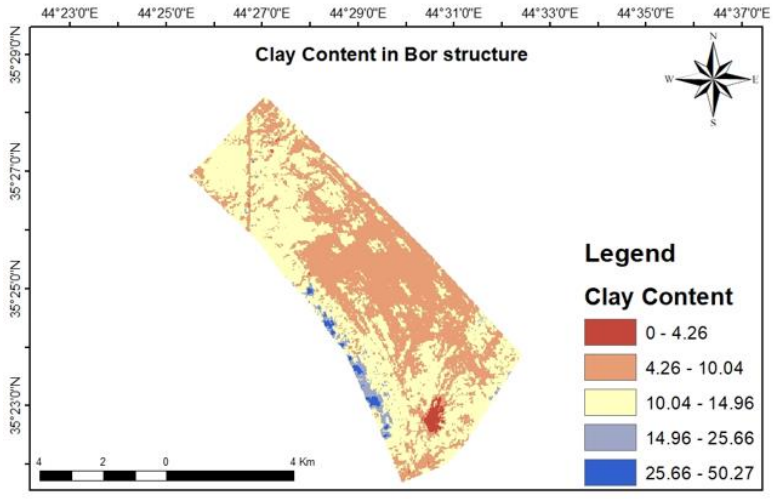


Fig. 17. Gird maps of clay content in Bor structure (using classification: Natural Breaks, 5 classes)

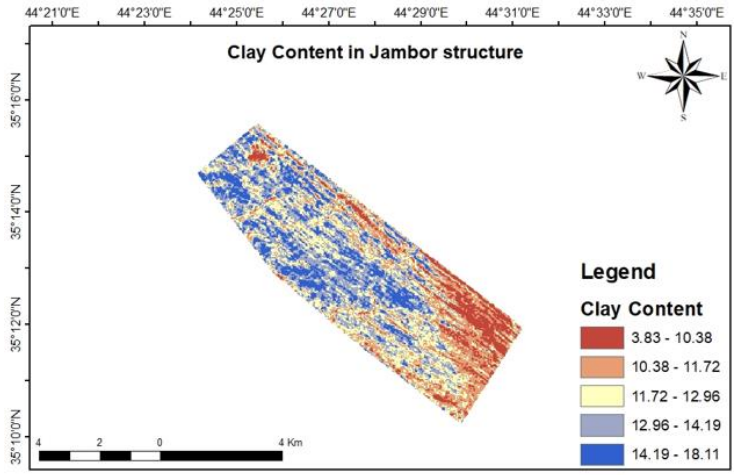


Fig. 18. Gird maps of clay content in Jambor structure (using classification: Natural Breaks, 5 classes)

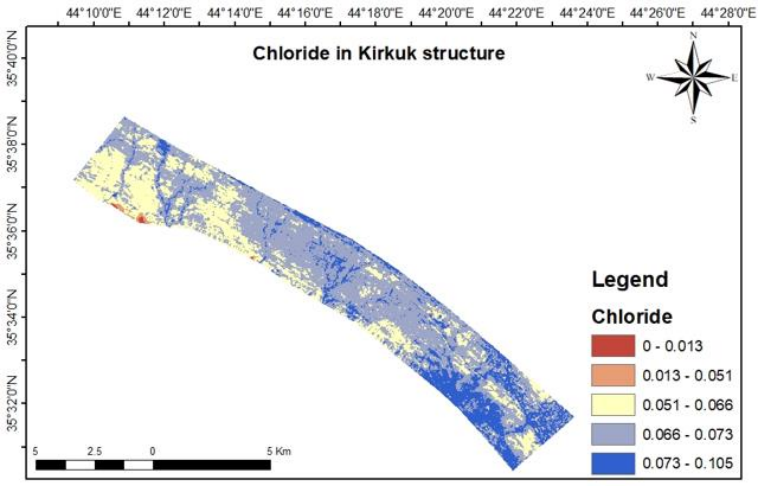


Fig. 19. Gird maps of chloride in Kirkuk structures (using classification: Natural Breaks, 5 classes)

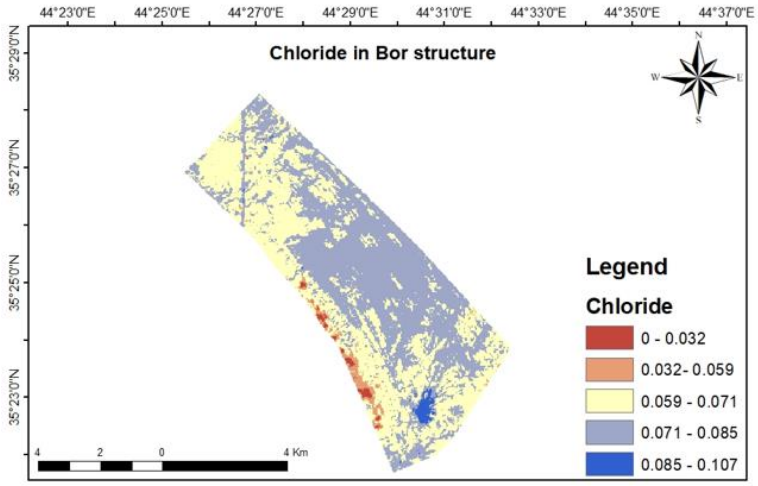


Fig. 20. Gird maps of chloride in Bor structures (using classification: Natural Breaks, 5 classes)

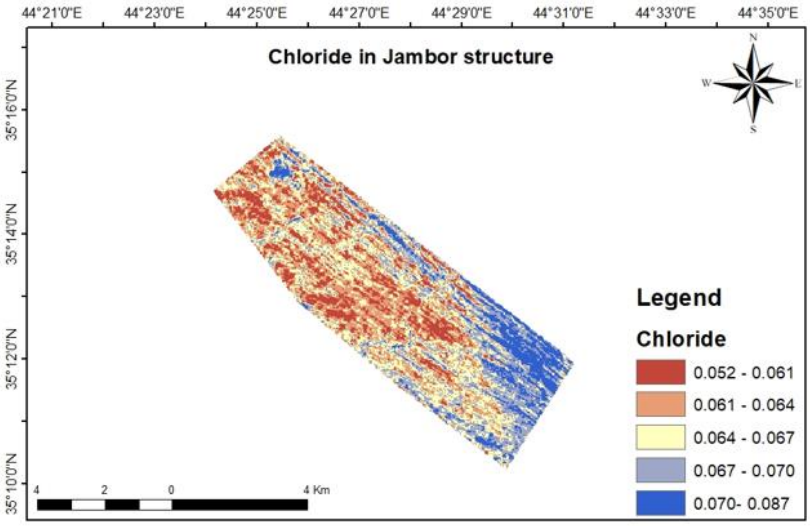


Fig. 21. Gird maps of chloride in Jambor structures (using classification: Natural Breaks, 5 classes)

4. Conclusions

A total of 52 soil samples were collected from the Fatha and Injana Formations for comprehensive analysis. Various aspects of the soil samples, including physical properties, chemical properties, regression analysis, and XRD, were examined to provide insights into the behavior of clay. The findings can be summarized as follows:

In the conducted study, an HS-5001EZ moisture density meter was utilized to measure the dry density of the soil samples, which ranged from 1.185 to 2.112 g/m^3. The dry density was observed to be lower in the Fatha Formation than in the Injana Formation. The silt content in all samples was found to be the highest, ranging from 28% to 93%. The plasticity index varied from low plastic to medium plastic.

The presence of gypsum layers in the Fatha Formation resulted in a higher gypsum content compared to other formations. A moderately positive correlation (R^2 = 0.702) was observed between chloride and EC. Additionally, a strong positive correlation was found between gypsum and sulfate (R^2 = 0.99), as well as between EC and TDS (R^2 = 0.99). The linear regression between chemical and physical properties yielded a low regression coefficient.

Applying multiple linear regression for clay properties proved to be appropriate, with regression coefficients ranging from 0.6 to 0.72. However, the nonlinear regression between clay characteristics produced significantly better results, with high regression coefficients. The SiO_2 content was observed to be high in all samples, ranging from 26.5% to 49.69%, and higher in the Fatha Formation than in the Injana Formation. The MgO content ranged from 4.224% to 8.868%, which was lower than that studied in the Injana Formation. The CaO content ranged from 11.85% to 23.95% and was present in carbonate form.

The XRD analysis revealed the presence of nonclay minerals such as quartz, feldspar, K-feldspar, calcite, and miscovite-calcite in the Injana Formation, while the Fatha Formation exhibited minerals such as quartz, feldspar, K-feldspar, calcite, calcite-dolomite, and gypsum-calcite. Clay minerals identified in the samples included chlorites-montmorillonite, illite, chlorites, illite-plygorskite, palygorskite, illite-muscovite, and gypsum. Quartz was found to be a widespread mineral in the clay samples.

Landsat images were employed to obtain data on inaccessible or remote areas, particularly for large regions. The correlation between clay properties and Landsat 8 data resulted in better results compared

to Landsat 7. A strong positive correlation was observed between gypsum and band 3 in Landsat 7. Clay exhibited a strong positive correlation with band 1 in Landsat 8, with a R^2 of 0.856.

Acknowledgements

The authors of this study wish to extend their sincere appreciation to the Geotechnic Materials Laboratory at Kirkuk Technical Engineering College for their invaluable support in conducting the necessary tests for this research.

References

Ahmed, C., Mohammed, A., Saboonchi, A., 2022. Arc GIS mapping, characterisations and modelling the physical and mechanical properties of the Sulaimani City soils, Kurdistan Region, Iraq. Geomechanics and Geoengineering, 17(2), 384-397.

Akumu, C., Johnson, J., Etheridge, D., Uhlig, P., Woods, M., Pitt, D., Mcmurray, S., 2015. Gis-fuzzy logic based approach in modeling soil texture: Using parts of the Clay Belt and Hornepayne region in Ontario Canada As A Case Study. Geoderma, 239, 13-24.

Al-Bassam, K. S., 2012. Mineral deposits and occurrences of the low folded zone. Iraqi Bulletin of Geology and Mining, (5), 159-188.

Al-Jaberi, M. H., Salim, L. N., 2022. Depositional properties of the Middle Miocene Fatha Formation, in K Oilfield, Southern Iraq. The Iraqi Geological Journal, 139-152.

Al-Juboury, A. I., Mccann, T., 2008. The Middle Miocene Fatha (Lower Fars) Formation, Iraq. Geoarabia, 13(3), 141-174.

Al-Juboury, A. I. A., 2009. The upper Miocene Injana (upper fars) formation of Iraq: Insights on provenance history. Arabian Journal Of Geosciences, 2, 337-364.

Al-Obeidi, A. H., Al-Jumaily, H. A., 2020. Geochemistry and environmental assessment of heavy metals in surface soil in Al-Hawija, southwest Kirkuk. The Iraqi Geological Journal, 36-61.

Alhirmizy, S., 2015. Automatic mapping of lineaments using shaded relief images derived from Digital Elevation Model (Dem) in Kirkuk Northeast Iraq. International Journal Science Resources, 4(5), 2228-2233.

Ali, A. R., Al-Mufti, T. M., Taqi, C. M., 2021. Geochemical distribution of some heavy metals in agricultural soil and their environmental impacts in Kirkuk, Northern Iraq. The Iraqi Geological Journal, 75-92.

Ali, M. H., Abood, M. R., Zarraq, G. A., 2023. Validity of the Injana Claystones as Fillers Al-Hajaj, Northern Salah-Alddin, Iraq. The Iraqi Geological Journal, 42-49.

Awadh, S. M., Awad, A. M., 2020. Manufacture of Portland cement from Late Miocene claystone, Injana formation, Central Iraq. Arabian Journal of Geosciences, 13(19), 1008.

Balasubramanian, P. A., 2017. Engineering properties of soils. Centre For Advanced Studies in Earth Science: University of Mysore, Mysore.

Brady, J. B., Newton, R. M., Boardman, S. J., 1995. New uses for powder X-Ray diffraction experiments in the undergraduate curriculum. Journal of Geological Education, 43(5), 466-470.

Buee, M., Courty, P.-E., Mignot, D., Garbaye, J., 2007. Soil niche effect on species diversity and catabolic activities in an ectomycorrhizal fungal community. Soil Biology and Biochemistry, 39(8), 1947-1955.

Da Silva Chagas, C., De Carvalho Junior, W., Bhering, S. B., Calderano Filho, B., 2016. Spatial prediction of soil surface texture in a semiarid region using random forest and multiple linear regressions. Catena, 139, 232-240.

Das, B. M., Sivakugan, N., 2015. Introduction to geotechnical engineering, Cengage Learning.

Dogan, H. M., 2009. Mineral composite assessment of kelkit River Basin in Turkey by means of remote sensing. Journal Of Earth System Science, 118, 701-710.

Dogan, H. M., Kılıç, O. M., 2013. Modelling and mapping some soil surface properties of Central Kelkit Basin in Turkey by using Landsat-7 Etm+ images. International Journal Of Remote Sensing, 34(15), 5623-5640.

Farquhar, S., Pearce, J., Dawson, G., Golab, A., Sommacal, S., Kirste, D., Biddle, D., Golding, S., 2015. A fresh approach to investigating Co2 storage: experimental Co2–water–rock interactions in a low-salinity reservoir system. Chemical Geology, 399, 98-122.

Goldsmith, W., Silva, M., Fischenich, J. C., 2001. determining optimal degree of soil compaction for balancing mechanical stability and plant growth capacity.

Grim, R. E., 1962. Applied Clay Mineralogy.

Hasan, S. F., Shareef, M. A., Hassan, N. D., 2021. Speckle filtering impact on land use/land cover classification area using the combination of Sentinel-1A and Sentinel-2B (a case study of Kirkuk City, Iraq). Arabian Journal Of Geosciences, 14(4), 276.

Hosseini, S. Z., Kappas, M., Bodaghabadi, M. B., Chahouki, M. A. Z., Khojasteh, E. R., 2014. Comparison of different geostatistical methods for soil mapping using remote sensing and environmental variables in Poshtkouh Rangelands, Iran. Polish Journal of Environmental Studies, 23(3), 737-751.

Hussein, M. L., Fadhil, L. A., Al-Mothen, A. A., 2021. Geochemical study of Injana Formation and its tectonic significances in selected areas, Iraq. The Iraqi Geological Journal, 41-52.

Ismail, N. R., Omar, H. M., 2014. Assessment of some clay deposits from Fatha Formation (M. Miocene) for brick manufacturing in Koya Area, Ne Iraq. Aro-The Scientific Journal of Koya University, 2(1), 16-23.

Jassim, S. Z., Goff, J. C., 2006. Geology of Iraq, Dolin, Sro, Distributed By Geological Society Of London.

Jobouri, M. A. J. A., 2005. Geochemistry of coloured argillites of Fatha Formation (Middle Miocene) and their industrial significance at selected areas in Northern Iraq. University Of Mosul.

Klein, K. A., Santamarina, J. C., 2003. Electrical conductivity in soils: Underlying Phenomena. Journal of Environmental Engineering Geophysics, 8(4), 263-273.

Liao, K., Xu, S., Wu, J., Zhu, Q., 2013. Spatial estimation of surface soil texture using remote sensing data. Soil Science and Plant Nutrition, 59(4), 488-500.

Lillesand, T., Kiefer, R. W., Chipman, J., 2015. Remote Sensing And Image Interpretation, John Wiley & Sons.

Maala, K., Sood, Q., Khames, D., Jabo, B., Al-Saade, N., Khadhum, M., 2007. Laboratory assessment for utilization of neogene mudstones in manufacturing of building bricks. Iraqi Bulletin of Geology and Mining, 3(2), 1-15.

Maarez, H. G., Jaber, H. S., Shareef, M. A., 2022. Utilization of geographic information system for hydrological analyses: a case study of Karbala province, Iraq. Iraqi Journal of Science, 4118-4130.

Martins, A. K., Gadiga, B. L., 2015. Satellite remote sensing for mineral deposit assessment of clay in Mubi Local Government Area Of Adamawa State, Nigeria. Geosciences, 5(1), 26-30.

Mcbratney, A. B., Santos, M. M., Minasny, B., 2003. On Digital Soil Mapping. Geoderma, 117(1-2), 3-52.

Mclean, E., 1983. Soil pH and lime requirement. methods of soil analysis: Part 2 Chemical and microbiological properties, 9, 199-224.

Mohammed, S. K., Al-Kubaisi, M. S., Bety, A. K., 2018. Heavy minerals distribution of Peramagroon Alluvial Fans Sulaimaniyah Governorate (Northern Iraq) as indicator to tectonic activity. Indian Journal of Natural Sciences, 9(51), 5679-15690.

Moreno-Maroto, J. M., Alonso-Azcárate, J., 2018. What is clay? A new definition of "clay" based on plasticity and its impact on the most widespread soil classification systems. Applied Clay Science, 161, 57-63.

Nanni, M. R., Demattê, J. A. M., 2006. Spectral reflectance methodology in comparison to traditional soil analysis. Soil Science Society of America Journal, 70(2), 393-407.

Nkwunonwo, U., Okeke, F., 2013. Gis-based production of digital soil map for Nigeria. Ethiopian Journal of Environmental Studies and Management, 6(5), 498-506.

Obaid, M. H., Kndhim, L. S., Salih, A. S. M., 2022. Mineralogy of Injana and recent sediments of selected areas in Salah Al-Din Governorate. AIP Conference Proceedings.

Polidori, E., 2007. Relationship between the Atterberg limits and clay content. Soils and foundations, 47(5), 887-896.

Raheem, A. M., Omar, N. Q., 2021. Investigation Of distinctive physico-chemical soil correlations for Kirkuk city using spatial analysis technique incorporated with statistical modeling. International Journal of Geo-Engineering, 12, 1-21.

Raheem, A. M., Omar, N. Q., Naser, I. J., Ibrahim, M. O., 2022. Gis implementation and statistical analysis for significant characteristics of Kirkuk soil. Journal of the Mechanical Behavior of Materials, 31(1), 691-700.

Salahalden, V. F., Shareef, M. A., Al Nuaimy, Q. A., 2023. Characterization of the chemical properties of deposited red clay soil using GIS based inverse distance weighted method in Kirkuk City, Iraq. Ecological Engineering Environmental Technology (Eeet), 24(7).

Saleh, A. M., 2017. Mineral Composite Assessment of Kerbala District in Iraq By Means Of Remote Sensing.

Scaramuzza, P. L., Bouchard, M. A., Dwyer, J. L., 2011. Development of the landsat data continuity mission cloud-cover assessment algorithms. IEEE Transactions on Geoscience and Remote Sensing, 50(4), 1140-1154.

Shahien, M., Ogila, W. A., 2022. Prediction of geotechnical properties of deltaic clays by using regression analysis models. Egyptian Journal of Pure and Applied Science, 59(2), 36-62.

Shareef, M., Hassan, N., Hasan, S., Khenchaf, A., 2020a. Integration of Sentinel-1A and Sentinel-2B Data for Land Use and Land Cover Mapping of the Kirkuk Governorate, Iraq. International Journal of Geoinformatics, 16(3).

Shareef, M. A., Ameen, M. H., Ajaj, Q. M., 2020b. Change detection and gis-based fuzzy ahp to evaluate the degradation and reclamation land of Tikrit City, Iraq. Geodesy And Cartography, 46(4), 194-203.

Shareef, M. A., Hasan, S. F., Ajaj, Q. M., 2018. Estimation and mapping of dates palm using Landsat-8 images: A case study in Baghdad City.International Conference On Advanced Science and Engineering (Icoase), 2018. Ieee, 425-430.

Shareef, M. A., Toumi, A., Khenchaf, A., 2014. Estimation of water quality parameters using the regression model with fuzzy k-means clustering. International Journal of Advanced Computer Science and Applications, 5(6).

Stevens, A., Udelhoven, T., Denis, A., Tychon, B., Lioy, R., Hoffmann, L., Van Wesemael, B., 2010. Measuring soil organic carbon in croplands at regional scale using airborne imaging spectroscopy. Geoderma, 158(1-2), 32-45.

Su, S. L., Singh, D. N., Baghini, M. S., 2014. A critical review of soil moisture measurement. Measurement, 54, 92-105.

Sulyman, M., Noori, A., Al-Attar, A., 2020. Study and Gis-based mapping of soil chemical properties in Kirkuk City, Iraq. Proceedings Of The 1st International Multi-Disciplinary Conference Theme: Sustainable Development And Smart Planning, Imdc-Sdsp 2020, Cyperspace, 28-30 June 2020.

Surdashy, A. A., Aqrawi, A. M., 2021. Assessment of clay deposits quality from East of Erbil, Kurdistan Region, Iraq for Some ceramic industries. The Iraqi Geological Journal, 145-161.

Taqi, A. H., Al Nuaimy, Q. A., Karem, G. A., 2016. Study of the properties of soil in Kirkuk, Iraq. Journal of Radiation Research and Applied Sciences, 9(3), 259-265.

Zhang, Y., Pu, S., Li, R. Y. M., Zhang, J., 2020. Microscopic and mechanical properties of undisturbed and remoulded red clay from Guiyang, China. Scientific Reports, 10(1), 18003.

Zovko, M., Romic, M., 2011. Soil contamination by trace metals: geochemical behaviour as an element of risk assessment. Earth and Environmental Sciences, 437-456.